



1 Seasonal variations and controlling factors of nitrogen 2 fluxes at the sediment-water interface in a semi-enclosed 3 inland sea

4 Zhaosen Wu^{1, 2}, Xinyu Guo^{2, *}, Jie Shi^{1, 3}, Xiaokun Ding⁴, Masatoshi Nakakuni^{5, 6},
5 Kuninao Tada^{5, 6}

6 ¹Key Laboratory of Marine Environment and Ecology, Ministry of Education of China, Ocean University
7 of China, 238 Songling Road, Qingdao 266100, China

8 ²Center for Marine Environmental Studies, Ehime University, 2-5 Bunkyo-Cho, Matsuyama 790-8577,
9 Japan

10 ³Laboratory for Marine Ecology and Environmental Sciences, Qingdao National Laboratory for Marine
11 Science and Technology, Qingdao, 266071, China

12 ⁴School of Ocean, Yantai University, Yantai, 264005, China

13 ⁵Faculty of Agriculture, Kagawa University, Ikenobe, Kita, Miki, Kagawa 761-0701, Japan

14 ⁶Seto Inland Sea Regional Research Center, Kagawa University, Saiwai, Takamatsu, Kagawa 761-0016,
15 Japan

16 Corresponding to: Xinyu Guo (guo.xinyu.mz@ehime-u.ac.jp) ORCID: 0000-0002-4832-8625

17

18 **Abstract.** Nitrogen fluxes across the sediment-water interface and nitrogen removal from sediments are
19 essential components of the nitrogen cycle and ecosystem in semi-enclosed inland seas. However, the
20 difficulty in observational sampling hinders the acquisition of continuous data necessary to understand
21 their seasonal variations and underlying mechanisms. In response to this issue, we have developed a one-
22 dimensional vertical model of the nitrogen cycle within sediments and used it to reproduce the seasonal
23 changes of observed nitrogen fluxes in a typical semi-enclosed inland sea and investigate their controlling
24 factors through sensitivity experiments. Model results indicate that 40% of particulate organic nitrogen
25 (PON) settling into sediments is returned to the bottom water as dissolved inorganic nitrogen (DIN),
26 while 30% is removed via N-loss flux (dinitrogen gas and nitrous oxide). Although PON flux is
27 controlled by PON concentration in the bottom water, DIN and N-loss fluxes show temperature-driven
28 seasonal variations, suggesting a decoupling between nitrogen return and PON input. Additionally,
29 seasonal variations in oxygen penetration depth (OPD), ranging from 1 to 3 mm, also affect nitrogen
30 fluxes. In nitrate-depleted sediments of semi-enclosed seas, the denitrification rate is no longer
31 significantly higher than the anammox rate in the nitrogen removal.



32 **Keywords:** sediment-water interface, semi-enclosed inland sea, nitrogen fluxes, sediment model,
33 nitrogen removal
34



35 1 Introduction

36 Sediments play a crucial role in regulating the storage and removal of nitrogen within semi-enclosed
 37 inland seas, which significantly influences the balance and stability of the ecosystem (Huettel et al., 2014;
 38 Zhang et al., 2020; Kalvelage et al., 2013; Thamdrup, 2012). On one hand, the sediment can bury
 39 substantial amounts of nitrogen, potentially on par with river inputs (Liu et al., 2021; Han et al., 2021;
 40 Lønborg and Markager, 2021). On the other hand, because of remineralization, the sediment
 41 continuously releases dissolved inorganic nitrogen (DIN) into the overlying water (Devol, 2015; Boynton
 42 et al., 2017; Liu et al., 2012). In the semi-enclosed inland sea, vertical mixing facilitates the contribution
 43 of DIN from sediments as a vital nutrient source for primary production because of shallow water depth
 44 (Huettel et al., 2014; Yi et al., 2023; Leng et al., 2023; Liu and Yin, 2007; Berelson et al., 2013; Leynaert
 45 et al., 2011; Mei Liu et al., 2011). Notably, the sediment serves as the primary anoxic environment in
 46 these regions, where key nitrogen removal processes, such as denitrification and anammox, occur. These
 47 processes are essential for regulating nitrogen inventories and influencing nutrient structure in these areas.
 48 Researches indicate that continental shelves, which constitute merely 7.5% of the global seafloor, are
 49 responsible for 44% of fixed nitrogen losses (Devol, 2015; Metigue et al., 2016; Huang et al., 2021; Jäntti
 50 and Hietanen, 2012; Khalil and Rasmussen, 2012). Furthermore, nitrous oxide, a byproduct of
 51 denitrification, is a significant greenhouse gas that contributes to global warming (Wilson et al., 2020;
 52 Yang et al., 2022).

53 To clarify the function of the sediment in ecological and environmental changes, it is necessary to
 54 conduct a quantitative analysis of nitrogen fluxes at the sediment-water interface in semi-enclosed inland
 55 seas, along with their seasonal variations. Direct observation of particulate organic nitrogen (PON) flux
 56 at this interface poses challenges due to the influence of resuspension processes. Consequently, numerous
 57 studies focused on DIN flux and its seasonal variations primarily through in situ observations, incubation
 58 experiments, or estimations based on Fick's law (De Vittor et al., 2012; Mu et al., 2017; Chen et al.,
 59 2023). For example, studies in the northern Adriatic Sea and the Baltic Sea have demonstrated the same
 60 conclusion that DIN flux exhibits seasonal variations, with higher levels in summer and lower levels in
 61 winter, likely influenced by water temperature (De Vittor et al., 2012; Niemistö et al., 2018). The fluxes
 62 of dinitrogen gas and nitrous oxide are mainly accessed through the measurement of denitrification and
 63 anammox rates within sediments (Zhang et al., 2018; Rich et al., 2020). A study conducted in the Pearl



64 River Estuary reported that the denitrification rate in sediments also displayed seasonal variability, with
65 peak values observed in summer and reduced values in winter (Teng and Lin, 2024). However, the
66 challenges and cost associated with field sampling limit the feasibility of continuous monitoring of these
67 fluxes. Moreover, the direction of DIN flux varies across different regions, with the underlying
68 mechanisms remaining unclear (Mu et al., 2017; De Vittor et al., 2015; Dale et al., 2022; Bohlen et al.,
69 2011; Ratmaya et al., 2022; Zhou et al., 2022). Therefore, identifying the magnitude and direction of
70 nitrogen fluxes at the sediment-water interface in semi-enclosed inland seas, along with their seasonal
71 patterns and underlying controlling mechanisms, is crucial for understanding the contribution of
72 sediments to the aquatic ecosystem in this region.

73 Numerical modeling is a valuable tool for understanding the factors that govern nitrogen fluxes at the
74 sediment-water interface. Typically, nitrogen fluxes at this interface derived from empirical formulas
75 serve as essential boundary conditions for modeling the aquatic nitrogen cycle in semi-enclosed inland
76 seas (Lønborg and Markager, 2021). However, this approach largely overlooks the changes occurring
77 within the sediment and the corresponding flux responses to these alterations. An alternative approach is
78 the implementation of a box model, which investigates nitrogen processes within the sediment.
79 Nonetheless, the box model's treatment of all sediment as a single domain, coupled with its failure to
80 account for the vertical distribution of chemical substances—particularly oxidants such as dissolved
81 oxygen (DO)—limits its capacity to provide a comprehensive understanding of the nitrogen cycling
82 processes within the sediment (Yang et al., 2022). A one-dimensional vertical sediment model addresses
83 this limitation, albeit at the cost of increased complexity and computational demands. This model has
84 demonstrated efficacy in accurately reproducing seasonal variations in nitrogen fluxes at the sediment-
85 water interface (Radtke et al., 2019; Umlauf et al., 2023). Despite the clear advantages of this modeling
86 approach over empirical formulas and box models, well-validated applications remain relatively scarce.
87 This study focuses on the unclear seasonal variations in the magnitude and direction of nitrogen fluxes
88 at the sediment-water interface in semi-enclosed inland seas, alongside the insufficiently understood
89 underlying mechanisms with controlling factors driving these changes. We developed a one-dimensional
90 vertical sediment model to simulate nitrogen cycling and accurately quantify nitrogen fluxes at the
91 interface. Supported by monthly continuous observations conducted in the sediment of Harima Nada in
92 Japan, a typical semi-enclosed inland sea, we obtained a robust dataset for model validation. The model

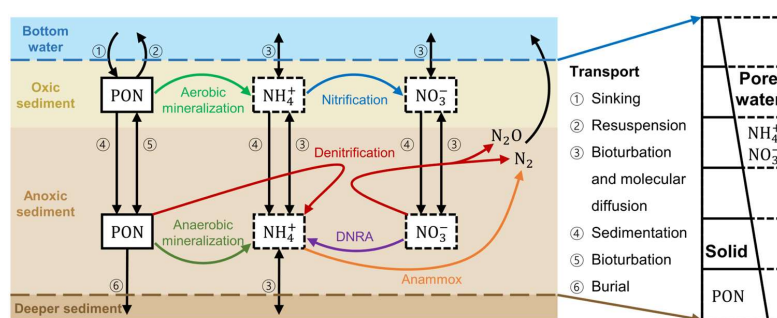


93 successfully reproduced the seasonal variations in the concentrations of three nitrogen species within the
 94 sediment and nitrogen fluxes at the interface. Additionally, numerical experiments further elucidated the
 95 influence of key environmental factors on these seasonal variations. This study aspires to establish a
 96 scientific foundation for comprehending the role of sediment nitrogen cycling in influencing the
 97 ecological environment of semi-enclosed marine systems. The findings can provide crucial support for
 98 offshore environmental remediation and the development of management policies.

100 2 Materials and Methods

101 2.1 Model descriptions

102 Based on the theory of early diagenesis (Berner, 1980), we have developed a biogeochemical model for
 103 sediment (Figure 1). This model encompasses two components: solid matter and pore water. The state
 104 variables consist of the concentrations of two types of PON (fast-decayed and slow-decayed ones) for
 105 the solid matter and the concentrations of NH_4^+ and NO_3^- in the pore water. Additionally, we set a fluff
 106 layer at the top of sediment, where the active benthos and material exchange processes with the above
 107 water column occur (Lee et al., 2002; Kuhrt et al., 2006; Laima et al., 2002).



108
 109 **Figure 1.** Physical and biogeochemical processes for nitrogen cycle in the sediment model. Three state variables in
 110 the model are PON, NH_4^+ and NO_3^- . PON is a solid substance (enclosed by solid lines), while NH_4^+ and NO_3^- are
 111 dissolved substances in the pore water (enclosed by dash lines). The physical processes and biogeochemical
 112 processes are denoted by black arrows and colored arrows, respectively. The numbers denote the transport processes
 113 included in the model.



114 In the solid part, the fast-decayed and slow-decayed PON are treated with a large and small
 115 mineralization rate, respectively. Both of them undergo identical vertical transport processes, including
 116 downward sedimentation driven by gravity and vertical diffusion caused by bioturbation. Their
 117 mineralization occurring within the sediment provides a flux of NH_4^+ into the pore water.
 118 In the pore water, the dissolved NH_4^+ and NO_3^- are transported downward and diffused vertically, as
 119 corresponding to both bioturbation and molecular diffusion. The biogeochemical processes occurring
 120 within the pore water include nitrification, denitrification, anammox and dissimilatory nitrate reduction
 121 to ammonium (DNRA).
 122 At the sediment-water interface, the exchange of solid matter is controlled by the bottom shear stress.
 123 The solid matter in the water column sinks into the fluff layer when the bottom stress is below a critical
 124 value, while resuspension occurs when the bottom stress exceeds this threshold. The exchange fluxes of
 125 NH_4^+ and NO_3^- at the interface are determined by the product of the diffusion coefficient and their
 126 concentration gradient between the fluff layer and the overlying water.
 127 In the deepest layer of sediment, only the slow-decayed PON is allowed to move downward and leave
 128 the model domain via burial. The exchange flux of NH_4^+ between the model domain and the underlying
 129 pore water is calculated by the production of the diffusion coefficient and the concentration gradient
 130 derived from observations, while the exchange flux of NO_3^- there is set to zero.

131 2.2 Equations and parameters

132 The equations for the concentrations of solid matter (C_s) and dissolved matter (C_d) are as follows:

$$133 \frac{\partial[(1-\phi) \cdot C_s]}{\partial t} = \frac{\partial[(1-\phi) \cdot D_B \frac{\partial C_s}{\partial z}]}{\partial z} - \frac{\partial[\omega \cdot (1-\phi) \cdot C_s]}{\partial z} + (1-\phi) \cdot \sum R_s \quad (1)$$

$$134 \frac{\partial[\phi \cdot C_d]}{\partial t} = \frac{\partial[\phi \cdot (D_B + D_M) \frac{\partial C_d}{\partial z}]}{\partial z} - \frac{\partial[\omega \cdot \phi \cdot C_d]}{\partial z} + \phi \cdot \sum R_d \quad (2)$$

135 Where z is vertical axis for sediment depth, t is time, ϕ is the sediment porosity, D_B and D_M are the
 136 bioturbation coefficient and molecular diffusion coefficient ($\text{m}^2 \text{s}^{-1}$), ω is the sedimentation rate
 137 (mm yr^{-1}), R_s is the biochemical reaction rate of PON, and R_d is the biochemical reaction rate of
 138 dissolved matter, including NH_4^+ and NO_3^- . Since the sediment type in the study area is muddy, the
 139 advection of pore water in sandy sediments controlled by pressure is neglected.

140 The vertical profile of D_B is expressed as equation (3) (Radtke et al., 2019).



$$D_B(z) = \begin{cases} D_{B_{\max}} & , 0 < z < z_{\max} \\ D_{B_{\max}} \cdot \exp\left(-\frac{z-z_{\max}}{z_d}\right) & , z \geq z_{\max} \end{cases} \quad (3)$$

Where z_{\max} is the depth down to which the maximum bioturbation coefficient ($D_{B_{\max}}$) is applied, z_d is the decaying length scale of $D_{B_{\max}}$.

D_M of dissolved matter in the pore water is a function of porosity, and is expressed as follows (Boudreau et al., 1998):

$$D_M(z) = \frac{D_0}{1 - 2.02 \ln(\theta)} \quad (4)$$

where D_0 is the diffusion coefficient of the dissolved matter in the particle-free liquid ($\text{m}^2 \text{s}^{-1}$).

The biochemical reactions are expressed in equations (5)-(7). Detailed descriptions of these reactions are presented in Table 1 (Soetaert et al., 1996; Capet et al., 2016; Akbarzadeh et al., 2018). These reaction equations primarily consider the limitations imposed by DO and temperature on each reaction. Due to the lack of parameterization schemes, it is difficult to represent the competition between different organisms for the same reaction. Since this is not the focus of this paper, we describe them collectively as a unified, generalized concept based on reaction rates. All the related coefficients and parameters are listed in Table 2. The sensitivity analysis of the model parameters is shown in Figure S1.

$$\sum R_{\text{PON}} = -R_{\min}^{O_2} - R_{\text{den}} - R_{\min}^{\text{AM}} - R_{\text{DNRA}} \quad (5)$$

$$\sum R_{\text{NH}_4^+} = R_{\min}^{O_2} + R_{\text{den}} + R_{\min}^{\text{AM}} + (1 + 0.5 \cdot r_{\text{C:N}}) R_{\text{DNRA}} - R_{\text{nit}} - R_{\text{Ana}} \quad (6)$$

$$\sum R_{\text{NO}_3^-} = R_{\text{nit}} - 0.5 \cdot r_{\text{C:N}} \cdot R_{\text{DNRA}} - 0.8 \cdot r_{\text{C:N}} \cdot R_{\text{den}} \quad (7)$$



159 **Table 1.** Reaction formulas and rate expressions.

Process	Formula	Rate expression
Aerobic mineralization	$(\text{CH}_2\text{O})_x(\text{NH}_3)_y(\text{H}_3\text{PO}_4)_z + x\text{O}_2$ $\rightarrow y\text{NH}_4^+ + x\text{H}_2\text{O}$	$R_{\min}^{\text{O}_2} = r_{\min} \cdot \text{PON} \cdot Q^{\frac{T-20}{10}}$ $\cdot \frac{\text{O}_2}{\text{O}_2 + K_{\text{S}_{\text{O}_2}}}$ $\cdot \frac{1}{\sum \text{lim}}$
Denitrification	$(\text{CH}_2\text{O})_x(\text{NH}_3)_y(\text{H}_3\text{PO}_4)_z + 0.8x\text{NO}_3^-$ $\rightarrow y\text{NH}_4^+ + 0.4x(1 - \alpha)\text{N}_2$ $+ 0.4x\alpha\text{N}_2\text{O} + 1.4x\text{H}_2\text{O}$	R_{den} $= r_{\min} \cdot \text{PON} \cdot Q^{\frac{T-20}{10}}$ $\cdot \frac{\text{NO}_3^-}{\text{NO}_3^- + K_{\text{S}_{\text{NO}_3^-}}}$ $\cdot \left(1 - \frac{\text{O}_2}{\text{O}_2 + K_{\text{in}_{\text{O}_2}^{\text{Den}}}}\right) \cdot \frac{1}{\sum \text{lim}} \cdot \gamma$
Anaerobic mineralization	$(\text{CH}_2\text{O})_x(\text{NH}_3)_y(\text{H}_3\text{PO}_4)_z + \text{an oxidant}$ $\rightarrow y\text{NH}_4^+ + x\text{ODU} + x\text{H}_2\text{O}$	R_{\min}^{AM} $= r_{\min} \cdot \text{PON} \cdot Q^{\frac{T-20}{10}}$ $\cdot \left(1 - \frac{\text{O}_2}{\text{O}_2 + K_{\text{in}_{\text{O}_2}^{\text{AM}}}}\right)$ $\cdot \left(1 - \frac{\text{NO}_3^-}{\text{NO}_3^- + K_{\text{in}_{\text{NO}_3^-}}}\right) \cdot \frac{1}{\sum \text{lim}}$
Nitrification	$\text{NH}_4^+ + 2\text{O}_2 \rightarrow \text{NO}_3^- + \text{H}_2\text{O}$	$R_{\text{nit}} = r_{\text{nit}} \cdot \text{NH}_4^+ \cdot \frac{\text{O}_2}{\text{O}_2 + K_{\text{S}_{\text{Nit}}}}$
DNRA	$(\text{CH}_2\text{O})_x(\text{NH}_3)_y(\text{H}_3\text{PO}_4)_z + 0.5x\text{NO}_3^-$ $\rightarrow (0.5x + y)\text{NH}_4^+$	R_{DNRA} $= r_{\min} \cdot \text{PON} \cdot Q^{\frac{T-20}{10}}$ $\cdot \frac{\text{NO}_3^-}{\text{NO}_3^- + K_{\text{S}_{\text{NO}_3^-}}}$ $\cdot \left(1 - \frac{\text{O}_2}{\text{O}_2 + K_{\text{in}_{\text{O}_2}^{\text{Den}}}}\right) \cdot \frac{1}{\sum \text{lim}}$ $\cdot (1 - \gamma)$
Anammox	$\text{NH}_4^+ + \text{NO}_2^- \rightarrow \text{N}_2 + 2\text{H}_2\text{O}$	$R_{\text{Ana}} = r_{\text{Ana}} \cdot \frac{\text{NH}_4^+}{\text{NH}_4^+ + K_{\text{S}_{\text{NH}_4^+}}}$ $\cdot \frac{\text{NO}_2^-}{\text{NO}_2^- + K_{\text{S}_{\text{NO}_2^-}}}$ $\cdot \frac{K_{\text{in}_{\text{O}_2}^{\text{Ana}}}}{\text{O}_2 + K_{\text{in}_{\text{O}_2}^{\text{Ana}}}}$



$$\Sigma \lim = \frac{O_2}{O_2 + K_{O_2}} + \frac{NO_3^-}{NO_3^- + K_{SNO_3^-}} \cdot \left(1 - \frac{O_2}{O_2 + K_{ln_{O_2}^{pen}}} \right) + \left(1 - \frac{O_2}{O_2 + K_{ln_{O_2}^{AM}}} \right) \cdot \left(1 - \frac{NO_3^-}{NO_3^- + K_{ln_{NO_3^-}}} \right). \quad x: y: z =$$

161 C: N: P.



162 **Table 2.** Model parameters.

Parameter	Value	Unit	Description	References
ω	2.6	mm yr ⁻¹	Sedimentation rate	(Ichimi et al., 2005)
$D_{B_{\max}}$	1.15×10^{-11}	m ² s ⁻¹	Maximum bioturbation coefficient	(Soetaert et al., 1996)
z_{\max}	0.01	m	Depth down to which the Maximum bioturbation coefficient is applied	(Soetaert et al., 1996)
z_d	0.5	m	Decaying length scale of the maximum bioturbation coefficient	(Soetaert et al., 1996)
$D_0^{NH_4^+}$	0.847	cm ² d ⁻¹	The molecular diffusion coefficient of ammonium in a particle-free solution at 0 °C	(Soetaert et al., 1996)
$D_0^{NO_3^-}$	0.845	cm ² d ⁻¹	The molecular diffusion coefficient of nitrate in a particle-free solution at 0 °C	(Soetaert et al., 1996)
$r_{\min f}$	2.8×10^{-9}	s ⁻¹	Mineralization rate of fast decay organic nitrogen	
$r_{\min s}$	1.05×10^{-9}	s ⁻¹	Mineralization rate of slow decay organic nitrogen	
Q	2		Factor for temperature effect on mineralization	(Capet et al., 2016)
$K_{S_{O_2}}$	3	μmol L ⁻¹	Half saturation constant of oxygen in aerobic mineralization	(Soetaert et al., 1996)



$K_{NO_3^-}$	30	$\mu\text{mol L}^{-1}$	Half saturation constant of nitrate in denitrification	(Soetaert et al., 1996)
$K_{O_2}^{\text{Den}}$	10	$\mu\text{mol L}^{-1}$	Half saturation constant of oxygen in denitrification	(Soetaert et al., 1996)
γ	95	%	Fraction of total nitrate Reduction occurring via denitrification	(Akbarzadeh et al., 2018)
$K_{O_2}^{\text{AM}}$	5	$\mu\text{mol L}^{-1}$	Half saturation constant of oxygen in anaerobic mineralization	(Soetaert et al., 1996)
$K_{NO_3^-}$	5	$\mu\text{mol L}^{-1}$	Half saturation constant of nitrate in anaerobic mineralization	(Soetaert et al., 1996)
r_{nit}	20	d^{-1}	Maximum nitrification rate	(Soetaert et al., 1996)
K_{nit}	1	$\mu\text{mol L}^{-1}$	Half saturation constant of oxygen in nitrification	(Soetaert et al., 1996)
r_{Ana}	2.3×10^{-4}	$\text{mmol m}^{-3} \text{ s}^{-1}$	Maximum anammox rate	(Akbarzadeh et al., 2018)
$K_{NH_4^+}$	5	$\mu\text{mol L}^{-1}$	Half saturation constant of ammonium in anammox	(Akbarzadeh et al., 2018)
$K_{NO_2^-}$	5	$\mu\text{mol L}^{-1}$	Half saturation constant of nitrite in anammox	(Akbarzadeh et al., 2018)
$K_{O_2}^{\text{Ana}}$	8	$\mu\text{mol L}^{-1}$	Half saturation constant of oxygen in anammox	(Akbarzadeh et al., 2018)



$r_{C:N}$	10.2		Ratio of carbon to nitrogen	
α	1	%	Nitrous oxide leakage during denitrification	(Akbarzadeh et al., 2018)
w	2	$m\ s^{-1}$	Sinking rate	(Ding et al., 2020)
τ_c	0.06	$N\ m^{-2}$	Critical bottom stress	(Ding et al., 2020)
E_{PON}	1×10^{-8}	$mmol\ m^{-2}\ s^{-1}$	Resuspension coefficient	(Ding et al., 2020)
D_{sur}	7×10^{-7}	$m^2\ s^{-1}$	Surface diffusion coefficient	(Radtke et al., 2019)
Δz	3	m	Distance of the diffusion layer at sediment-water interface	(Nakakuni et al., 2024)



Due to the large biomass of benthos and high DO concentrations in the fluff layer, the mineralization rate in this layer is set to be 50 times faster than that in the sediment below it (Lee et al., 2002; Kuhrt et al., 2006; Laima et al., 2002).

At the sediment-water interface, the sinking and resuspension of PON depend on the bottom stress. The exchange flux (F_s) is expressed as (Wang, 2002):

$$F_s = \begin{cases} w \cdot C_s^w \cdot \left(\frac{\tau}{\tau_c} - 1\right), & \tau < \tau_c \\ E_s \cdot \left(\frac{\tau}{\tau_c} - 1\right), & \tau \geq \tau_c \end{cases} \quad (8)$$

where w is the sinking velocity of particles in the bottom water (m s^{-1}), C_s^w is concentration of PON in the bottom water (mmol m^{-3}), τ is the bottom stress (N m^{-2}), τ_c is the critical bottom stress (N m^{-2}), E_s is the resuspension rate ($\text{mmol m}^{-2} \text{s}^{-1}$).

The exchanges of dissolved matters (NH_4^+ and NO_3^-) are mainly through bioturbation and molecular diffusion, and the flux (F_d) is expressed as (Boudreau et al., 1998):

$$F_d = -D_{\text{sur}} \cdot \phi \cdot \frac{C_d^w - C_d^{\text{pw}}}{\Delta z} \quad (9)$$

where D_{sur} is the surface diffusion coefficient ($\text{m}^2 \text{s}^{-1}$). C_d^w and C_d^{pw} are the concentrations of dissolved matter in the bottom water and pore water of fluff layer, respectively (mmol m^{-3}). Δz is the distance of the diffusion layer at sediment-water interface (m).

At the bottom of the model domain, the slow-decayed PON is allowed to move out as the burial process with a flux (B_s) as (Radtke et al., 2019):

$$B_s = \omega \cdot (1 - \phi) \cdot C_s^b \quad (10)$$

where superscript of b represents the deepest layer of the model domain.

The bottom flux of NH_4^+ (B_d) is expressed as:

$$B_d = -(D_B^b + D_M^b) \cdot \phi \cdot \frac{C_d^b - C_d^{\text{bc}}}{\Delta z^b} \quad (11)$$

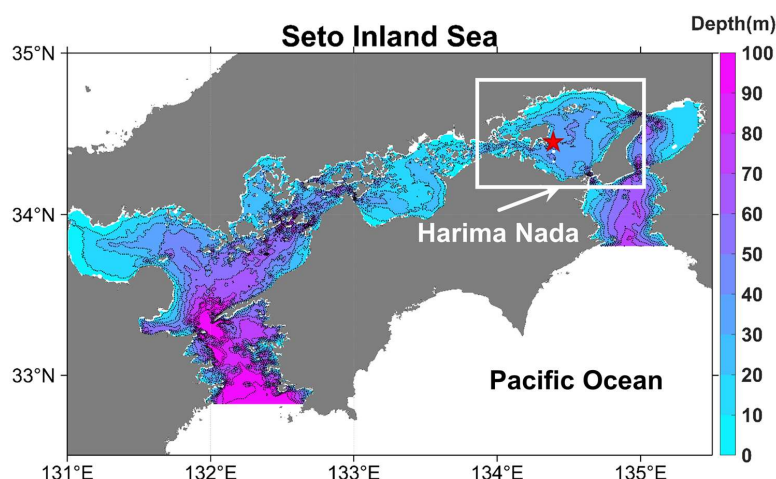
where C_d^{bc} is NH_4^+ concentration in the pore water under the deepest layer of the model domain (mmol m^{-3}).

2.3 Study area

Harima Nada is situated within Seto Inland Sea, the largest semi-enclosed sea in Japan (Figure 2). It has an average water depth of 26 meters and is connected to Osaka Bay and Hiuchi Nada on the eastern and western sides, respectively. To the south, it connects to the Pacific Ocean through the Naruto Strait and



191 Kii Channel (Zhu et al., 2019; Chang et al., 2009). Over the past few decades, the environment of the
 192 Seto Inland Sea has undergone significant changes (Ishii et al., 2014; Yamamoto et al., 2021). With the
 193 continuous observations of sediments in Harima Nada by our collaborators, we have realized that the
 194 DIN input from sediments in this area is comparable to that from rivers, exhibiting notable seasonal
 195 variations (Leng et al., 2023; Nakakuni et al., 2024). However, the driving factors and mechanisms
 196 behind these seasonal changes remain unclear. Therefore, Harima Nada serves as an excellent study area,
 197 and these observational data can provide a sufficient validation to ensure the reliability of model results
 198 (Nakakuni et al., 2024). This allows us to analyze the seasonal variations in sediment nitrogen cycling
 199 and interfacial nitrogen fluxes, as well as their controlling mechanisms. Additionally, this study lays the
 200 groundwork for future exploration of how sediment nitrogen cycling responds to long-term changes in
 201 the aquatic environment.



202
 203 **Figure 2.** Study area of the Harima Nada, Japan. The red star represents the site where the observational data used
 204 in this study were collected.

205 2.4 Model configurations

206 Since this study focuses on seasonal changes at the sediment–water interface, the sediment depth in the
 207 model was set to 10 cm and uniformly divided into 100 layers.

208 The initial concentrations of the four state variables were obtained from the core observations in Harima
 209 Nada in July 2020 (Nakakuni et al., 2024). Moreover, the observed profile of DO concentration (Sayama



et al., 2002), nitrite (NO_2^-) concentration, and porosity were also included and always constant in the model as input condition (Figure S2c-e and Text S2). Monthly observations of bottom water temperature and concentrations of PON, NH_4^+ , and NO_3^- from February 2020 to January 2021 were used to prescribe the upper boundary conditions, while NH_4^+ concentration beneath the model domain from April 2020 to May 2021 served as the bottom boundary conditions (Nakakuni et al., 2024). The bottom stress was derived from a hydrodynamic model for the Seto Inland Sea (Zhu et al., 2019) (Figure 3). Forced by these boundary conditions, the sediment model was calculated for a long time (more than 500 years) to reach a steady-state condition, wherein the input and output fluxes of materials become balanced.

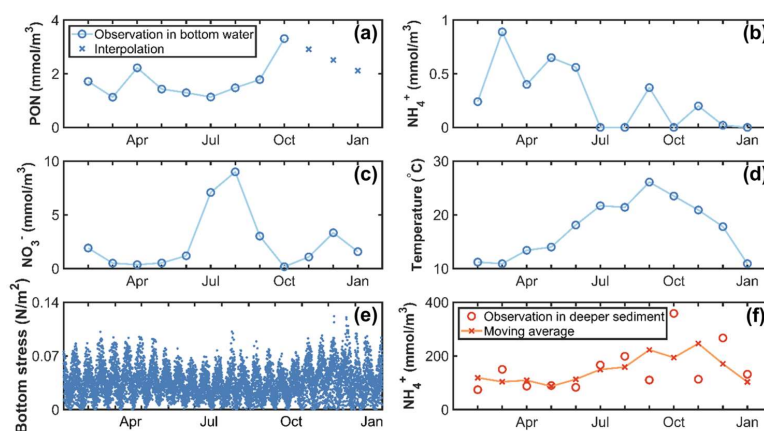


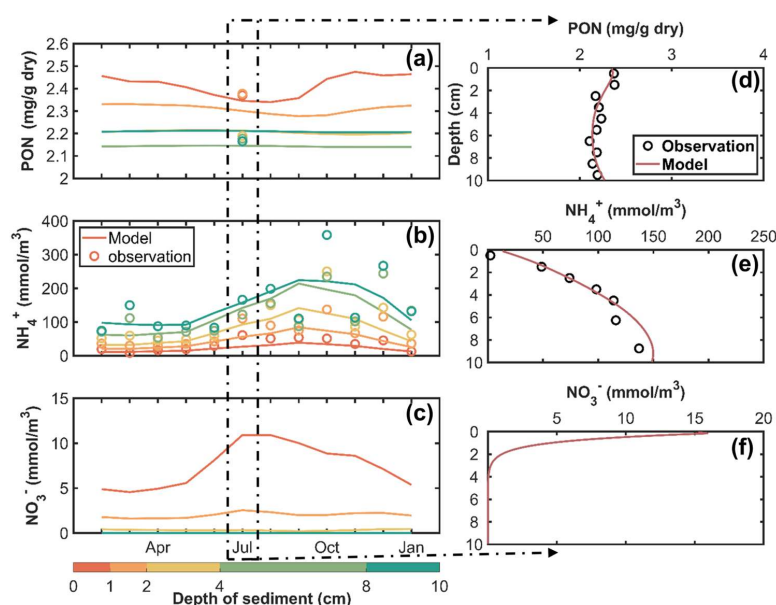
Figure 3. Boundary conditions of the model: (a) PON concentration, (b) NH_4^+ concentration, (c) NO_3^- concentration in the bottom water, (d) bottom water temperature, (e) bottom stress and (f) NH_4^+ concentration in the layer below model domain (10-12 cm). The values of PON concentration in the bottom water from November to January are obtained by linear interpolation. A three-point moving average is applied to NH_4^+ concentrations in (f) to smooth out intra-seasonal fluctuations.



226 3 Results

227 3.1 Seasonal variations of the particle and dissolved nitrogen concentrations in the sediment

228 The monthly concentrations of PON, NH_4^+ and NO_3^- at different layers from 0 to 10 cm in the model
 229 domain are shown in Figure 4, alongside the corresponding observed data. The comparison between the
 230 model results and the observations, especially for the data in July (Figure 4d-e), suggests a reliable
 231 performance of the model.



232 **Figure 4.** The seasonal variations of concentrations of (a) PON, (b) NH_4^+ and (c) NO_3^- in different layers in the
 233 sediment, the vertical profiles of (d) PON, (e) NH_4^+ and (f) NO_3^- in July. Colors in (a)-(c) represent different depth.
 234 In all the panels, lines are model results and circles are the observation data.
 235

236 The concentration of PON in the sediment was consistently greater in the surface layer compared to the
 237 underlying layers (Figure 4a). Its seasonal variation was apparent in the upper 3 cm of sediment and
 238 almost disappears in the layers below 3 cm. In the 0-1 cm layer, PON concentration decreased from a
 239 value of 2.46 mg/g in February to a minimum value of 2.34 mg/g in August, followed by an increase to
 240 a peak concentration of 2.47 mg/g in November. In the deep layer of the sediment (8-10 cm), PON
 241 concentration remained around 2.20 mg/g throughout the year.

242 The NH_4^+ concentration had a minimum value at the surface and a maximum value at the deepest layer
 243 (Figure 4b), which was contrary to the vertical distribution of PON concentrations. The NH_4^+



concentrations presented significant seasonal variations across entire sediment layers, with the range of variation increasing with depth. For example, the NH_4^+ concentration in the 0-1 cm layer presented the lowest value of $11.02 \text{ mmol m}^{-3}$ in February and the highest value of $38.71 \text{ mmol m}^{-3}$ in September; however, the NH_4^+ concentration in the deep layer of the sediment (8-10 cm) presented the lowest value of $90.97 \text{ mmol m}^{-3}$ in April and the highest value of $224.34 \text{ mmol m}^{-3}$ in September. Except for the episodic high values observed in the deep sediment layer during autumn, the model successfully reproduced the seasonal variation of NH_4^+ concentration across all sediment layers, which was characterized by lower levels in winter and spring and elevated levels in summer and autumn. NO_3^- concentration reached its peak at the sediment surface and exhibited a rapid decline to zero at the depth of around 3 cm (Figure 4c and f). Its seasonal variation occurred within the upper 1 cm layer, showing a high value in summer. The maximum concentration in the 0-1 cm layer was $10.91 \text{ mmol m}^{-3}$ in July, which was double the minimum concentration of 4.56 mmol m^{-3} in March.

3.2 The flux of PON, DIN and N-loss (N_2 and N_2O) between bottom water and sediment

PON sank from the bottom water to the sediment throughout the year (Figure 5a). PON flux was high in fall with the maximum value of $2.90 \text{ mmol m}^{-2} \text{ d}^{-1}$ in October and low in spring with the minimum value of $1.07 \text{ mmol m}^{-2} \text{ d}^{-1}$ in May.

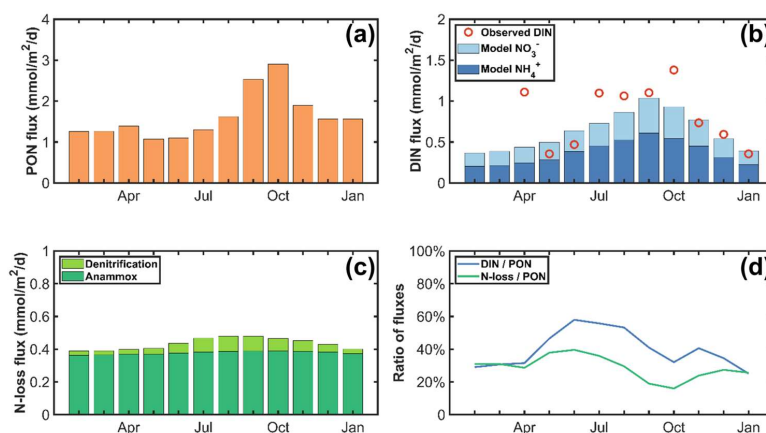


Figure 5. The fluxes of (a) PON, (b) DIN, (c) N-loss (N_2 and N_2O) at the sediment-water interface in the model, and (d) the ratios of DIN and N-loss fluxes to PON flux. The red circles in (b) are the values given by observations.



263 The fluxes of NH_4^+ and NO_3^- was summed up to account the flux of DIN between bottom water and
 264 sediment. DIN in the Harima Nada was released from the sediment into the bottom water throughout the
 265 year, exhibiting the highest flux of $1.04 \text{ mmol m}^{-2} \text{ d}^{-1}$ in September and the lowest flux of $0.37 \text{ mmol m}^{-2} \text{ d}^{-1}$ in February (Figure 5b). The DIN flux and its seasonal variation given by the model exhibit a general
 266 agreement with observations (Nakakuni et al., 2024), although the model does not capture the observed
 267 high flux in April. The NH_4^+ and NO_3^- fluxes demonstrated comparable seasonal trends, reaching their
 268 respective maxima in September (0.61 and $0.43 \text{ mmol m}^{-2} \text{ d}^{-1}$) and minima in February (0.20 and 0.16
 269 $\text{mmol m}^{-2} \text{ d}^{-1}$).

271 N-loss is produced through denitrification and anammox inside the sediment, which releases N_2 and N_2O
 272 to the atmosphere. N-loss flux across the sediment-water interface reached its peak of $0.48 \text{ mmol m}^{-2} \text{ d}^{-1}$
 273 in August and the lowest value of $0.39 \text{ mmol m}^{-2} \text{ d}^{-1}$ in February (Figure 5c). The anammox was the
 274 main process for producing N_2 and contributed a value of around $0.37 \text{ mmol m}^{-2} \text{ d}^{-1}$ to N_2 flux, with
 275 minimal seasonal variation. Conversely, denitrification contributed to a seasonal variation of N-loss flux,
 276 reaching a maximum of $0.09 \text{ mmol m}^{-2} \text{ d}^{-1}$ in August and a minimum of $0.03 \text{ mmol m}^{-2} \text{ d}^{-1}$ in March.
 277 Although N_2 was the main product of denitrification, the flux of N_2O , a potent greenhouse gas, was not
 278 negligible. It varied from 0.3 to $0.9 \text{ } \mu\text{mol m}^{-2} \text{ d}^{-1}$, with a mean value of $0.55 \text{ } \mu\text{mol m}^{-2} \text{ d}^{-1}$.

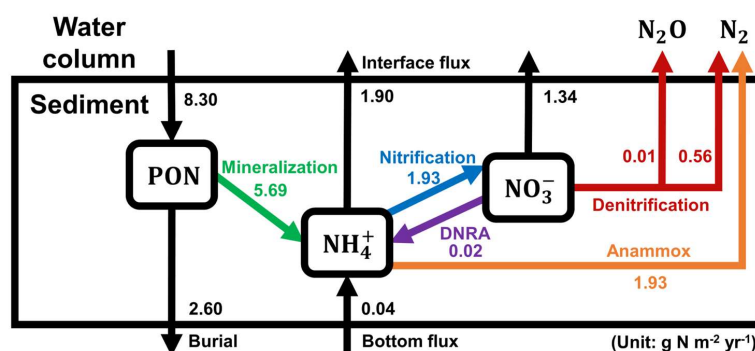
279 The ratio of DIN flux to PON flux ($R_{\text{DIN/PON}}$) reflects the fraction of nitrogen that sinks into the sediment
 280 and later releases back to the seawater (Figure 5d). $R_{\text{DIN/PON}}$ increased from 25% in January to a peak of
 281 58% in June, with the annual average of 40%. The ratio of N-loss flux to PON flux ($R_{\text{N-loss/PON}}$)
 282 represented the proportion of nitrogen removed from the sediment. The highest value of $R_{\text{N-loss/PON}}$ was
 283 40% in June while the lowest value was 16% in October. The sum of $R_{\text{DIN/PON}}$ and $R_{\text{N-loss/PON}}$ ranged from
 284 48% in October to 98% in June, with an annual average of 69%. It suggested that around 30% of the
 285 PON flux sinking from seawater was retained in the sediment on average, with this retention rate
 286 potentially reaching nearly 50% during certain months.

287 3.3 The budgets of PON, NH_4^+ and NO_3^- in the sediment

288 The annual budgets for the three forms of nitrogen in the sediment of Harima Nada are estimated from
 289 the model results (Figure 6). The sinking of PON from bottom water was the source of PON in the
 290 sediment, quantified at $8.30 \text{ g N m}^{-2} \text{ yr}^{-1}$. Since the primary production in the Harima Nada in 2020 was



291 estimated to be $41 \text{ g N m}^{-2} \text{ yr}^{-1}$ (Tada, 2021), it could be interpreted that about 20% of the particles
 292 produced by primary production sank into the sediment. Within the deeper layers of the sediment, the
 293 burial rate of PON was $2.60 \text{ g N m}^{-2} \text{ yr}^{-1}$, representing 31% of the PON flux into the sediment and 6% of
 294 the primary production. The rest $5.69 \text{ g N m}^{-2} \text{ yr}^{-1}$ of PON flux into the sediment was mineralized to
 295 NH_4^+ , which became the main source of NH_4^+ in the sediment.



296
 297 **Figure 6.** Nitrogen budgets in the sediment model of Harima Nada.

298 In addition to mineralization, DNRA also produced NH_4^+ in our model, but its value of $0.02 \text{ g N m}^{-2} \text{ yr}^{-1}$
 299 ¹ was two orders of magnitude lower than the amount of mineralization ($5.69 \text{ g N m}^{-2} \text{ yr}^{-1}$). And 0.04 g
 300 $\text{N m}^{-2} \text{ yr}^{-1}$ of NH_4^+ was supplied from the deeper sediment located beneath the model domain.
 301 Furthermore, NH_4^+ has three sinks: the nitrification of NH_4^+ to NO_3^- had a rate of $1.93 \text{ g N m}^{-2} \text{ yr}^{-1}$,
 302 the anammox of NH_4^+ to N_2 had a rate of $1.93 \text{ g N m}^{-2} \text{ yr}^{-1}$, and the upward NH_4^+ flux through the
 303 sediment-water interface was quantified at $1.90 \text{ g N m}^{-2} \text{ yr}^{-1}$.
 304 For the NO_3^- produced by the nitrification, it mainly had an upward flux of $1.34 \text{ g N m}^{-2} \text{ yr}^{-1}$ at the
 305 sediment-water interface and the denitrification of $0.57 \text{ g N m}^{-2} \text{ yr}^{-1}$. The combined effects of
 306 denitrification of NO_3^- and anammox of NH_4^+ produced a N-loss flux to the atmosphere amounting to
 307 $2.50 \text{ g N m}^{-2} \text{ yr}^{-1}$ (2.49 for N_2 and 0.01 for N_2O). Since this value represented over 30% of PON sinking
 308 flux to the sediment, it became an important process for removing nitrogen in the semi-enclosed inland
 309 sea.

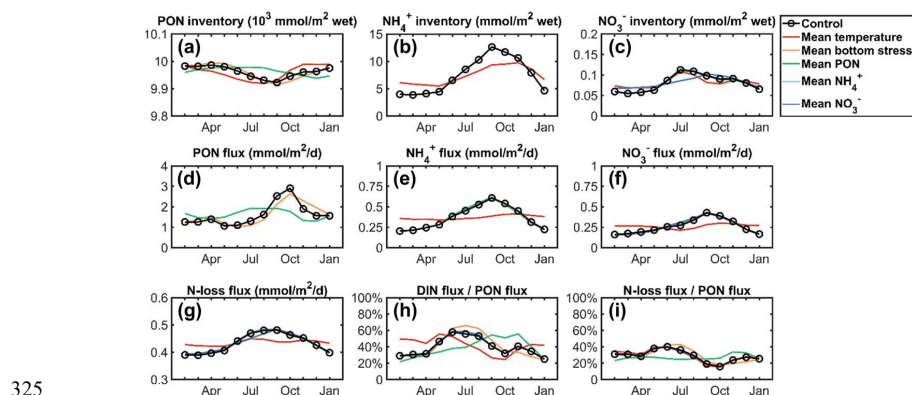


310 4 Discussion

311 4.1 Factors affecting the seasonal variations in the sediment-water fluxes of nitrogen

312 The model results show that the fluxes of PON, DIN and N-loss between seawater and sediment exhibit
 313 apparent seasonal variations. To clarify the factors controlling these seasonal variations, we carried out
 314 five sensitivity experiments, in which we removed the seasonal variation of one of the following five
 315 variables by substituting its monthly means with its annual mean: PON concentration (PON^{bw}), NH_4^+
 316 concentration ($\text{NH}_4^{+\text{bw}}$), NO_3^- concentration ($\text{NO}_3^{-\text{bw}}$), bottom water temperature, and bottom stress.
 317 Figure 7 shows the calculation results of the five sensitivity experiments alongside the results described
 318 in Section 3 (referred to “Control” in Figure 7).

319 The concentration of PON^{bw} and the bottom water temperature significantly influence the seasonal
 320 variation of PON inventory in the sediment (Figure 7a). Sinking of PON^{bw} serves as the source of PON
 321 in the sediment, while variations in bottom water temperature can change the mineralization rate in the
 322 sediment (Figure S3a and Text S3). Although these seasonal variations can directly impact the PON
 323 inventory, the extent of seasonal variation in PON inventory is relatively minor, with its value being
 324 more than two orders of magnitude smaller than the overall PON inventory.



325 **Figure 7.** Comparisons of the model results among six calculations (five sensitivity experiments and one control
 326 run). The sensitivity experiments include the cases removing the seasonal variations of PON concentration (green
 327 line, “Mean PON”), NH_4^+ concentration (light blue, “Mean NH_4^+ ”), NO_3^- concentration (dark blue, “Mean NO_3^- ”),
 328 and water temperature (red line, “Mean temperature”) in the overlying water, as well as of the bottom stress (orange
 329 line, “Mean bottom stress”). (a) PON inventory; (b) NH_4^+ inventory; (c) NO_3^- inventory; (d) PON flux; (e) NH_4^+
 330 flux; (f) NO_3^- flux; (g) N-loss flux; (h) ratio of DIN flux to PON flux; (i) ratio of N-loss flux to PON flux.



332 Among the 5 factors, only the bottom water temperature is responsible for the seasonal variations of
 333 NH_4^+ inventory (Figure 7b) as it affects the mineralization rate that produces NH_4^+ in the sediment
 334 (Figure S3 and Text S3). The seasonal variation of NO_3^- inventory is mainly controlled by $\text{NO}_3^{-\text{bw}}$
 335 instead of bottom water temperature (Figure 7c). When the concentration of $\text{NO}_3^{-\text{bw}}$ is fixed at its annual
 336 mean, a decrease in concentration enhances an increase in NO_3^- flux from the sediment to the overlying
 337 water (Figure 7f), leading to a corresponding decline in NO_3^- inventory (Figure S4 and Text S4).
 338 The seasonal variation in concentration of PON^{bw} is the main factor deciding the seasonal variation of
 339 PON flux across the interface between the bottom water and sediment (Figure 7d). High concentration
 340 of PON^{bw} leads to an increased sinking flux of PON from seawater to sediment. With the annual
 341 average value of PON^{bw} concentration as the input condition, the peak PON flux from the seawater to
 342 sediment in October disappears (Figure 3a). In such a case, an inverse seasonal relationship can be
 343 discerned between PON flux (the green line in Figure 7d) and bottom stress (Figure 3e). The rise in
 344 bottom stress during the spring and winter induces the resuspension of PON at the sediment-water
 345 interface, thereby diminishing the downward PON flux.
 346 The bottom water temperature controls not only the seasonal variations of NH_4^+ inventory in the
 347 sediment (Figure 7b) but also that of NH_4^+ flux from the sediment to the bottom water (Figure 7e). This
 348 is because NH_4^+ concentration in the sediment is much higher than the concentration of $\text{NH}_4^{+\text{bw}}$, and its
 349 variation directly determines the change of NH_4^+ flux (Figure 3b and Figure 4b). Since NH_4^+ is the sole
 350 source of NO_3^- in the sediment by nitrification (Figure 6 and Figure S3b), NO_3^- flux is consequently
 351 controlled by the bottom water temperature (Figure 7f). As a combination of NH_4^+ flux and NO_3^- flux,
 352 the seasonal variation of DIN flux is also controlled by the bottom water temperature, which is consistent
 353 with the conclusion suggested from field studies (Nakakuni et al., 2024).
 354 The differences in the factors controlling the seasonal variation of PON and DIN fluxes indicate that a
 355 large PON flux into the sediment does not necessarily lead to a corresponding increase in DIN flux from
 356 the sediment to the bottom water. This suggests that estimating the DIN flux by using reflective boundary
 357 conditions based only on the concentration of PON^{bw} , or relying on empirical formulations that neglect
 358 bottom water temperature, may lead to considerable inaccuracies in the representing of the seasonal
 359 variation in DIN flux.



360 N-loss occurs through denitrification and anammox, and is consequently closely associated with the
 361 inventories of NH_4^+ and NO_3^- in the sediment. Our calculation shows that the seasonal variation in N-
 362 loss flux mainly depends on the bottom water temperature and NO_3^{bw} (Figure 7g). Since anammox is
 363 the dominant process for producing N_2 in the sediment, the bottom temperature, rather than NO_3^{bw} , has
 364 a greater impact on the seasonal variation of N-loss flux.

365 $R_{\text{DIN/PON}}$ and $R_{\text{N-loss/PON}}$ are two important parameters for comprehending the nitrogen cycle in the semi-
 366 enclosed inland sea. The seasonal variation of $R_{\text{DIN/PON}}$ is likely controlled by PON^{bw} and bottom
 367 temperature (Figure 7h). The annual mean of bottom temperature appears to advance the peak of $R_{\text{DIN/PON}}$,
 368 whereas the annual mean of PON^{bw} delays this peak. Conversely, $R_{\text{N-loss/PON}}$ is only affected by PON^{bw}
 369 (Figure 7i). The absence of an effect from bottom temperature effect on $R_{\text{N-loss/PON}}$ is caused by the
 370 relatively smaller range of N-loss flux compared to PON flux.

371 4.2 Influences of the DO profiles on nitrogen cycle in the sediment

372 The availability of DO has an important impact on the nitrogen cycle in the pore water. The DO
 373 concentration has a maximum value at the top of the pore water and diminishes with increasing depths
 374 (Devol, 2015). Consequently, the vertical profile of DO concentration in the sediment is characterized
 375 by a surface maximum concentration (DO_{max}) and the oxygen penetration depth (OPD). To assess the
 376 sensitivity of our model results to the specified DO concentration in the sediment, we conducted two
 377 groups of numerical experiments to clarify the effects of DO_{max} (GROUP I) and OPD (GROUP II) on
 378 the nitrogen cycle in the sediment.

379 According to the observed data obtained from the Ministry of the Environment of Japan (<https://water-pub.env.go.jp/water-pub/mizu-site/mizu/kouiki/dataMap.asp>), the average concentration of DO in the
 380 bottom water in the Seto Inland Sea ranged from 429 to 714 mmol m^{-3} in the past 40 years, which is far
 381 beyond the DO concentration in the fluff layer as the input data (84 mmol m^{-3}). Therefore, in GROUP I
 382 of the numerical experiments, DO_{max} was varied within the range of 60-140 mmol m^{-3} , while OPD was
 383 maintained at a constant value of 2 mm. The model results showed that there were no significant changes
 384 in the nitrogen inventories of the three types of nitrogen or their fluxes at the sediment-water interface
 385 (figures not given). The reason is that DO is not a limiting factor for nitrogen cycle within the aerobic
 386 zone of the upper 3 mm of sediment when DO_{max} is maintained between 60-140 mmol m^{-3} .
 387



It has been reported that the OPD in inland sediment can reach around 5 mm (Dale et al., 2011). In the five simulations of GROUP II, OPD was changed from 1 to 5 mm in 1 mm increments, while DO_{max} was maintained at a constant level of 80 mmol m^{-3} . The vertical profiles of DO concentration were derived through exponential fitting. The model results indicated that OPD has clear influences on NO_3^- inventory, NH_4^+ flux, NO_3^- flux and N-loss flux (Figures 8c, e, f, g). An increase of OPD facilitates the occurrence of nitrification in an expanded aerobic zone, leading to a greater conversion of NH_4^+ to NO_3^- . Since NH_4^+ mainly remains in the deeper sediment layers (Figure 4b), nitrification occurring in the surface sediment has a minimal impact on NH_4^+ inventory (Figure 8b). However, it can significantly reduce NH_4^+ flux at the sediment-water interface (Figure 8e). NO_3^- inventory in the sediment increases by 218% as OPD rises from 1 to 5 mm (Figure 8c). The increase in NO_3^- inventory subsequently enhances both NO_3^- flux and denitrification, resulting in a higher N-loss flux (Figures 8f and g). However, there is minimal difference in the NH_4^+ , NO_3^- , and N-loss fluxes among the cases with OPD values of 3, 4, and 5 mm, indicating that beyond a certain critical threshold, the influence of OPD on these fluxes becomes negligible. Therefore, if the OPD exhibits seasonal variation between 1 and 3 mm, it will have a significant impact on the seasonal variation of nitrogen fluxes; if the OPD remains consistently deeper than 3 mm, its impact is less pronounced. Moreover, since an increase in OPD has opposing effects on NH_4^+ and NO_3^- fluxes, its overall influence on DIN flux is minimal.

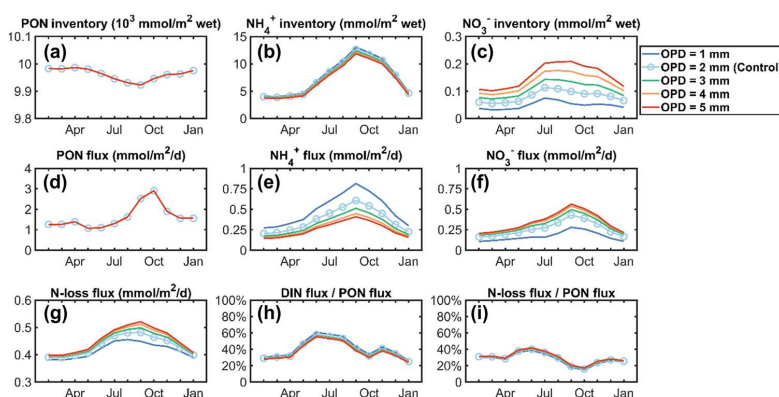


Figure 8. The effect of OPD depth on the nitrogen cycle in sediment: (a) PON inventory; (b) NH_4^+ inventory; (c) NO_3^- inventory; (d) PON flux; (e) NH_4^+ flux; (f) NO_3^- flux; (g) N-loss flux; (h) ratio of DIN flux to PON flux; (i) ratio of N-loss to PON flux.



409 **4.3 Comparisons with other coastal seas**

410 Numerous studies have evaluated the nitrogen fluxes at the sediment-water interface, yielding varying
411 conclusions (Zhou et al., 2017; Sun et al., 2021; Canion et al., 2014; Lin et al., 2017; De Vittor et al.,
412 2012; Mu et al., 2017; Rich et al., 2020; Dale et al., 2022; Bohlen et al., 2011; Ratmaya et al., 2022;
413 Zhou et al., 2022). In this subsection, we compare the fluxes of NH_4^+ , NO_3^- and N-loss calculated by
414 our sediment model with the values reported in these studies for different coastal seas (Table 3).

415



416 **Table 3.** Benthic fluxes ($\text{mmol m}^{-2} \text{d}^{-1}$) reported in some regions; positive values represent the release from sediment
 417 to water.

Flux	Value		Location	References
NH_4^+	1.53	to 1.62	Northern Adriatic Sea	(De Vittor et al., 2012)
	0.16	to 1.39	Mauritanian upwelling region	(Dale et al., 2022)
	0.12	to 5.3	Vilaine Bay	(Ratmaya et al., 2022)
	-0.1077	to 0.219	Areas off eastern Taiwan	(Zhou et al., 2017)
	-0.71	to 0.14	Bohai Bay	(Mu et al., 2017)
	-0.1	to 0.066	Yellow Sea and East China Sea	(Zhou et al., 2022)
	0	to 4	Peruvian upwelling region	(Bohlen et al., 2011)
	0.0867	to 0.4722	Taranto Gulf	(De Vittor et al., 2015)
	0.22	to 0.63	Harima Nada	This study
NO_3^-	-0.46	to -0.26	Northern Adriatic Sea	(De Vittor et al., 2012)
	-3	to -0.1	Mauritanian upwelling region	(Dale et al., 2022)
	-0.62	to 0.46	Vilaine Bay	(Ratmaya et al., 2022)
	-0.241	to 0.00005	Areas off eastern Taiwan	(Zhou et al., 2017)
	1.43	to 2.26	Bohai Bay	(Mu et al., 2017)
	-3.43	to 0.082	Yellow Sea and East China Sea	(Zhou et al., 2022)
	-3.8	to -0.3	Peruvian upwelling region	(Bohlen et al., 2011)
	4.8	to 8.8	Taranto Gulf	(De Vittor et al., 2015)
	0.17	to 0.43	Harima Nada	This study
N_2	2.7	to 544.3	Chinese marginal seas	(Sun et al., 2021)



28.70	to 420.49	East China Sea	(Lin et al., 2017)
0.2	to 2.8	Arctic shelf	(Canion et al., 2014)
1322.4	to 2683.2	Peru margin	(Rich et al., 2020)
0.40	to 0.48	Harima Nada	This study

418



419 NH_4^+ is released from the sediment to the bottom water in our study area. It is commonly observed and
 420 has been reported in other coastal regions, including Northern Adriatic Sea (De Vittor et al., 2012),
 421 Vilaine Bay (Ratmaya et al., 2022) and Eastern Taiwan (Zhou et al., 2017). The difference between our
 422 study area and these coastal waters is that the sediment in our region also serves as a source of NO_3^- for
 423 the overlying seawater. The NO_3^- concentrations observed in the bottom water of Harima Nada were not
 424 always higher than that in the pore water. Consequently, NO_3^- produced by nitrification in the sediment
 425 can be released into the water column. In contrast, in areas such as the offshore of eastern Taiwan, the
 426 sediment continuously absorbs NO_3^- from the overlying water because of the lower concentration of
 427 NO_3^- in the pore water compared to the overlying water (Zhou et al., 2017).

428 The N-loss flux is an important sink of nitrogen in the sediment of the Harima Nada, constituting about
 429 30% of the sinking flux of PON into the sediment. The flux of N_2 estimated in our study is about one to
 430 two orders of magnitude smaller than the values reported in other areas such as the East China Sea and
 431 Arctic shelf. This discrepancy may be attributed to higher bacterial activity in those areas or to elevated
 432 concentrations of organic matter and NO_3^- in the sediment (Sun et al., 2021; Canion et al., 2014; Lin et
 433 al., 2017; Rich et al., 2020).

434 Our results indicate that the anammox rate is approximately three times greater than the denitrification
 435 rate. However, some previous studies reported that anammox contributes a smaller N_2 flux compared to
 436 denitrification (Teng and Lin, 2024; Dalsgaard et al., 2005). The first reason for this difference is the
 437 lower maximum NO_3^- concentration or shallower NO_3^- penetration in Harima Nada sediments, which
 438 leads to a denitrification rate lower than that in those regions. In addition, the low concentration of NH_4^+
 439 in the sediment of those regions, even as the same scale as the NO_3^- concentration, limits the rate of
 440 anammox and reduces the contribution to N_2 . In contrast, NH_4^+ concentration in the sediment in this
 441 study was significantly higher than NO_3^- concentration, thereby enhancing the potential rate of
 442 anammox (Canion et al., 2014; Rich et al., 2020). Another reason is that the sediment thickness utilized
 443 in our model was set at 10 cm, whereas most conventional observations sampled only the surface
 444 sediment, potentially underestimating the contribution of anammox in deeper layers. Usually, NH_4^+
 445 concentrations in pore water are much lower in the surface layer compared to deeper layers, resulting in
 446 a reduced anammox reaction rate in the 0–5 cm layer relative to the 5–10 cm layer. When concentrating
 447 on the upper 5 cm of sediment, our model results suggest that the anammox rate constitutes a smaller



448 proportion of N_2 , accounting for less than 50% in summer (Figure S5 and Text S5), which is consistent
 449 with some observations (Teng and Lin, 2024; Dalsgaard et al., 2005).

450

451 **5 Conclusions**

452 This study developed a one-dimensional vertical sediment model to investigate the seasonal variations
 453 in the direction and magnitude of nitrogen fluxes at the sediment-water interface in semi-enclosed inland
 454 seas, and to reveal the controlling mechanisms of various environmental factors on these variations.
 455 Utilizing continuous observational data from a typical semi-enclosed inland sea for validation, we found
 456 that the flux of PON settling from the bottom water to the sediment is the main source of nitrogen in the
 457 sediment, with its seasonal variation governed by the PON concentration in the bottom water. Due to the
 458 regeneration of a substantial amount of NH_4^+ in the sediment, NH_4^+ is continuously released from the
 459 sediment to the overlying water, with its seasonal variation being temperature-controlled. Temperature
 460 influences the mineralization rate, which subsequently affects NH_4^+ flux through NH_4^+ inventory in the
 461 sediment. NO_3^- flux at the interface is directed upward in an oligotrophic water column, and its seasonal
 462 variation is also temperature-controlled. The influence of temperature over NH_4^+ inventory in the
 463 sediment is transmitted to NO_3^- inventory through nitrification, thereby affecting NO_3^- flux. This results
 464 in the seasonal variation of DIN flux returning from the sediment to the water being unrelated to the PON
 465 flux, as these two are controlled by different environmental factors with distinct seasonal patterns. This
 466 finding suggests that neglecting to consider bottom water temperature and PON concentration in
 467 reflective boundary conditions or empirical formulas may lead to varying degrees of misestimation when
 468 calculating the seasonal variation of DIN flux at the sediment-water interface.

469 The rate of nitrogen removal in sediments with low nitrate levels, possibly found in oligotrophic
 470 environments, is primarily controlled by anammox. Moreover, traditional observations are limited by the
 471 sampling depth of sediments, which may result in an underestimation of the contribution of anammox in
 472 deeper sediment layers. Our findings indicate that the maximum concentration of DO in sediments, which
 473 ranged from 60 to 140 $mmol\ m^{-3}$, has a negligible impact on sediment nitrogen cycling. However,
 474 seasonal variations in oxygen penetration depth, which ranges from 1 to 3 mm, can significantly influence
 475 nitrogen fluxes at the sediment-water interface. In addition, this model is mainly suited for semi-enclosed



476 inland seas dominated by muddy sediments and does not account for the advection of pore water flow in
477 sandy sediments. In practice, this process can be incorporated by adjusting the vertical velocity in the
478 solute transport equation. Overall, this model can be widely applied to investigate nitrogen cycling-
479 related issues in nearshore muddy sediments. Moreover, by investigating the seasonal variations of
480 nitrogen cycling in semi-enclosed inland sea sediments and their controlling factors, it can provide a
481 basis for governance and management support for environmental issues such as coastal eutrophication.
482 In future research, we will expand upon this study by integrating it with long-term observational data to
483 investigate the effects of prolonged changes in aquatic environments, such as eutrophication and seawater
484 warming, on sediment nitrogen cycling and nitrogen flux at the sediment-water interface.

485

486 **Code, data, or code and data availability**

487 The source code of the numerical model used in this study is available on request. Please contact the
488 corresponding author.

489

490 **Author contributions**

491 Zhaosen Wu: conceptualization, methodology, software, validation, visualization, writing (original draft
492 preparation). Xinyu Guo: formal analysis, methodology, resources, supervision, writing (review and
493 editing). Jie Shi: supervision, writing (review and editing). Xiaokun Ding: methodology, software.
494 Masatoshi Nakakuni: data curation, investigation, resources. Kuninao Tada: data curation, investigation,
495 resources.

496

497 **Competing interests**

498 The authors declare that they have no conflict of interest.

499



500 **Supporting Information**

501 Supporting Information is available free of charge at the Biogeosciences website.

502

503 **Acknowledgement**

504 This research was performed by the Environment Research and Technology Development Fund
505 (JPMEERF20255002) of the Environmental Restoration and Conservation Agency Provided by the
506 Ministry of Environment of Japan. We thank Dr. Akihiko Morimoto and Dr. Naoki Yoshie who worked
507 in the Center for Marine Environmental Studies, Ehime University, Japan and provided valuable
508 suggestions for our research. Z. Wu thanks the China Scholarship Council (CSC) and the Ministry of
509 Education, Culture, Sports, Science and Technology, Japan (MEXT) for a project on Joint
510 Usage/Research Center, Leading Academia in Marine and Environmental Research (LaMer) for
511 supporting his study in Japan.

512

513



514 **References**

- 515 Akbarzadeh, Z., Laverman, A. M., Rezanezhad, F., Raimonet, M., Viollier, E., Shafei, B., and Van
 516 Cappellen, P.: Benthic nitrite exchanges in the Seine River (France): An early diagenetic modeling
 517 analysis, *Sci Total Environ*, 628-629, 580-593, 10.1016/j.scitotenv.2018.01.319, 2018.
- 518 Berelson, W. M., McManus, J., Severmann, S., and Reimers, C. E.: Benthic flux of oxygen and nutrients
 519 across Oregon/California shelf sediments, *Cont. Shelf Res.*, 55, 66-75, 10.1016/j.csr.2013.01.009, 2013.
- 520 Berner, R.: Early diagenesis: a theoretical approach: Princeton, 1980.
- 521 Bohlen, L., Dale, A. W., Sommer, S., Mosch, T., Hensen, C., Noffke, A., Scholz, F., and Wallmann, K.:
 522 Benthic nitrogen cycling traversing the Peruvian oxygen minimum zone, *Geochim. Cosmochim. Acta*,
 523 75, 6094-6111, 10.1016/j.gca.2011.08.010, 2011.
- 524 Boudreau, B. P., Mucci, A., Sundby, B., Luther, G. W., and Silverberg, N.: Comparative diagenesis at
 525 three sites on the Canadian continental margin, *J. Mar. Res.*, 56, 1259-1284,
 526 10.1357/002224098765093634, 1998.
- 527 Boynton, W. R., Ceballos, M. A. C., Bailey, E. M., Hodgkins, C. L. S., Humphrey, J. L., and Testa, J.
 528 M.: Oxygen and Nutrient Exchanges at the Sediment-Water Interface: a Global Synthesis and Critique
 529 of Estuarine and Coastal Data, *Estuaries Coasts*, 41, 301-333, 10.1007/s12237-017-0275-5, 2017.
- 530 Canion, A., Overholt, W. A., Kostka, J. E., Huettel, M., Lavik, G., and Kuypers, M. M.: Temperature
 531 response of denitrification and anaerobic ammonium oxidation rates and microbial community structure
 532 in Arctic fjord sediments, *Environ Microbiol*, 16, 3331-3344, 10.1111/1462-2920.12593, 2014.
- 533 Capet, A., Meysman, F. J. R., Akoumianaki, I., Soetaert, K., and Grégoire, M.: Integrating sediment
 534 biogeochemistry into 3D oceanic models: A study of benthic-pelagic coupling in the Black Sea, *Ocean*
 535 *Modelling*, 101, 83-100, 10.1016/j.ocemod.2016.03.006, 2016.
- 536 Chang, P.-H., Guo, X., and Takeoka, H.: A numerical study of the seasonal circulation in the Seto Inland
 537 Sea, Japan, *Journal of Oceanography*, 65, 721-736, 10.1007/s10872-009-0062-4, 2009.
- 538 Chen, S., Gao, D., Zhang, J., Zheng, Y., Li, X., Dong, H., Yin, G., Han, P., Liang, X., Liu, M., Müller,
 539 C., and Hou, L.: Gross nitrogen transformations in intertidal sediments of the Yangtze Estuary:
 540 Distribution patterns and environmental controls, *Geoderma*, 429, 10.1016/j.geoderma.2022.116233,
 541 2023.



542 Dale, A. W., Clemens, D., Dähnke, K., Korth, F., Wankel, S. D., Schroller-Lomnitz, U., Wallmann, K.,
 543 and Sommer, S.: Nitrogen cycling in sediments on the NW African margin inferred from N and O
 544 isotopes in benthic chambers, *Frontiers in Marine Science*, 9, 10.3389/fmars.2022.902062, 2022.

545 Dale, A. W., Sommer, S., Bohlen, L., Treude, T., Bertics, V. J., Bange, H. W., Pfannkuche, O., Schorp,
 546 T., Mattsdotter, M., and Wallmann, K.: Rates and regulation of nitrogen cycling in seasonally hypoxic
 547 sediments during winter (Boknis Eck, SW Baltic Sea): Sensitivity to environmental variables, *Estuar.*
 548 *Coast. Shelf Sci.*, 95, 14-28, 10.1016/j.ecss.2011.05.016, 2011.

549 Dalsgaard, T., Thamdrup, B., and Canfield, D. E.: Anaerobic ammonium oxidation (anammox) in the
 550 marine environment, *Research in microbiology*, 156, 457-464, 2005.

551 De Vittor, C., Relitti, F., Kralj, M., Covelli, S., and Emili, A.: Oxygen, carbon, and nutrient exchanges
 552 at the sediment–water interface in the Mar Piccolo of Taranto (Ionian Sea, southern Italy), *Environmental*
 553 *Science and Pollution Research*, 23, 12566-12581, 10.1007/s11356-015-4999-0, 2015.

554 De Vittor, C., Faganeli, J., Emili, A., Covelli, S., Predonzani, S., and Acquavita, A.: Benthic fluxes of
 555 oxygen, carbon and nutrients in the Marano and Grado Lagoon (northern Adriatic Sea, Italy), *Estuarine,*
 556 *Coastal and Shelf Science*, 113, 57-70, 10.1016/j.ecss.2012.03.031, 2012.

557 Devol, A. H.: Denitrification, Anammox, and N₂ Production in Marine Sediments, *Annu. Rev. Mar. Sci.*,
 558 7, 403-423, 10.1146/annurev-marine-010213-135040, 2015.

559 Ding, X., Guo, X., Zhang, C., Yao, X., Liu, S., Shi, J., Luo, C., Yu, X., Yu, Y., and Gao, H.: Water
 560 conservancy project on the Yellow River modifies the seasonal variation of Chlorophyll-a in the Bohai
 561 Sea, *Chemosphere*, 254, 126846, 10.1016/j.chemosphere.2020.126846, 2020.

562 Han, A., Kao, S. J., Lin, W., Lin, Q., Han, L., Zou, W., Tan, E., Lai, Y., Ding, G., and Lin, H.: Nutrient
 563 Budget and Biogeochemical Dynamics in Sansha Bay, China: A Coastal Bay Affected by Intensive
 564 Mariculture, *Journal of Geophysical Research: Biogeosciences*, 126, 10.1029/2020jg006220, 2021.

565 Huang, F., Lin, X., Hu, W., Zeng, F., He, L., and Yin, K.: Nitrogen cycling processes in sediments of the
 566 Pearl River Estuary: Spatial variations, controlling factors, and environmental implications, *CATENA*,
 567 206, 105545, <https://doi.org/10.1016/j.catena.2021.105545>, 2021.

568 Huettel, M., Berg, P., and Kostka, J. E.: Benthic Exchange and Biogeochemical Cycling in Permeable
 569 Sediments, *Annu. Rev. Mar. Sci.*, 6, 23-51, 10.1146/annurev-marine-051413-012706, 2014.



570 Ichimi, K., Tada, K., and Montani, S.: The phytoplankton assemblage of the past and present in the Seto
 571 Inland Sea-the expectation from sediment core samples, *Aquabiology*, 27, 214~221, 2005.

572 Ishii, D., Yanagi, T., and Sasakura, S.: Long-term trends in the occurrence of red tides in the Seto Inland
 573 Sea, Japan, *Oceanography in Japan*, 23, 217-236, 10.5928/kaiyou.23.6_217, 2014.

574 Jäntti, H. and Hietanen, S.: The Effects of Hypoxia on Sediment Nitrogen Cycling in the Baltic Sea,
 575 *Ambio*, 41, 161-169, 10.1007/s13280-011-0233-6, 2012.

576 Kalvelage, T., Lavik, G., Lam, P., Contreras, S., Arteaga, L., Löscher, C. R., Oschlies, A., Paulmier, A.,
 577 Stramma, L., and Kuypers, M. M. M.: Nitrogen cycling driven by organic matter export in the South
 578 Pacific oxygen minimum zone, *Nature Geoscience*, 6, 228-234, 10.1038/ngeo1739, 2013.

579 Khalil, M. A. K. and Rasmussen, R. A.: The global sources of nitrous oxide, *Journal of Geophysical*
 580 *Research: Atmospheres*, 97, 14651-14660, 10.1029/92jd01222, 2012.

581 Kuhrts, C., Seifert, T., and Fennel, W.: Modeling Transport of Fluff Layer Material in the Baltic Sea,
 582 *Hydrobiologia*, 554, 25-30, 10.1007/s10750-005-1003-x, 2006.

583 Laima, M., Maksymowska-Brossard, D., Sauriau, P.-G., Richard, P., Girard, M., Gouleau, D., and
 584 Joassard, L.: Fluff deposition on intertidal sediments: effects on benthic biota, ammonium fluxes and
 585 nitrification rates, *Biogeochemistry*, 61, 115-133, 10.1023/a:1020264414924, 2002.

586 Lee, J.-Y., Tett, P., Jones, K., Jones, S., Luyten, P., Smith, C., and Wild-Allen, K.: The PROWQM
 587 physical-biological model with benthic-pelagic coupling applied to the northern North Sea, *J. Sea Res.*,
 588 48, 287-331, [https://doi.org/10.1016/S1385-1101\(02\)00182-X](https://doi.org/10.1016/S1385-1101(02)00182-X), 2002.

589 Leng, Q., Guo, X., Zhu, J., and Morimoto, A.: Contribution of the open ocean to the nutrient and
 590 phytoplankton inventory in a semi-enclosed coastal sea, *Biogeosciences*, 20, 4323-4338, 10.5194/bg-20-
 591 4323-2023, 2023.

592 Leynaert, A., Longphuiert, S. N., An, S., Lim, J.-H., Claquin, P., Grall, J., Kwon, B. O., and Koh, C. H.:
 593 Tidal variability in benthic silicic acid fluxes and microphytobenthos uptake in intertidal sediment,
 594 *Estuarine, Coastal and Shelf Science*, 95, 59-66, 10.1016/j.ecss.2011.08.005, 2011.

595 Lin, X., Liu, M., Hou, L., Gao, D., Li, X., Lu, K., and Gao, J.: Nitrogen Losses in Sediments of the East
 596 China Sea: Spatiotemporal Variations, Controlling Factors, and Environmental Implications, *Journal of*
 597 *Geophysical Research: Biogeosciences*, 122, 2699-2715, 10.1002/2017jg004036, 2017.



- 598 Liu, H. and Yin, B.: Annual cycle of carbon, nitrogen and phosphorus in the Bohai Sea: A model study,
 599 Cont. Shelf Res., 27, 1399-1407, 10.1016/j.csr.2007.01.015, 2007.
- 600 Liu, S. M., Li, L. W., Zhang, G. L., Liu, Z., Yu, Z., and Ren, J. L.: Impacts of human activities on nutrient
 601 transports in the Huanghe (Yellow River) estuary, Journal of Hydrology, 430-431, 103-110,
 602 10.1016/j.jhydrol.2012.02.005, 2012.
- 603 Liu, X., Stock, C. A., Dunne, J. P., Lee, M., Shevliakova, E., Malyshev, S., and Milly, P. C. D.: Simulated
 604 Global Coastal Ecosystem Responses to a Half-Century Increase in River Nitrogen Loads, Geophysical
 605 Research Letters, 48, e2021GL094367, <https://doi.org/10.1029/2021GL094367>, 2021.
- 606 Lønborg, C. and Markager, S.: Nitrogen in the Baltic Sea: Long-term trends, a budget and decadal time
 607 lags in responses to declining inputs, Estuarine, Coastal and Shelf Science, 261, 107529,
 608 <https://doi.org/10.1016/j.ecss.2021.107529>, 2021.
- 609 McTigue, N. D., Gardner, W. S., Dunton, K. H., and Hardison, A. K.: Biotic and abiotic controls on co-
 610 occurring nitrogen cycling processes in shallow Arctic shelf sediments, Nature Communications, 7,
 611 13145, 10.1038/ncomms13145, 2016.
- 612 Mei Liu, S., Wei Li, L., and Zhang, Z.: Inventory of nutrients in the Bohai, Cont. Shelf Res., 31, 1790-
 613 1797, 10.1016/j.csr.2011.08.004, 2011.
- 614 Mu, D., Yuan, D., Feng, H., Xing, F., Teo, F. Y., and Li, S.: Nutrient fluxes across sediment-water
 615 interface in Bohai Bay Coastal Zone, China, Mar. Pollut. Bull., 114, 705-714,
 616 10.1016/j.marpolbul.2016.10.056, 2017.
- 617 Nakakuni, M., Yamaguchi, H., Ichimi, K., and Tada, K.: Seasonal variation in pore water nutrients and
 618 their fluxes from the bottom sediments in Harima Nada, Seto Inland Sea, Journal of Oceanography, 80,
 619 219-232, 10.1007/s10872-024-00719-7, 2024.
- 620 Niemistö, J., Kononets, M., Ekeröth, N., Tallberg, P., Tengberg, A., and Hall, P. O. J.: Benthic fluxes of
 621 oxygen and inorganic nutrients in the archipelago of Gulf of Finland, Baltic Sea – Effects of sediment
 622 resuspension measured in situ, J. Sea Res., 135, 95-106, 10.1016/j.seares.2018.02.006, 2018.
- 623 Radtke, H., Lipka, M., Bunke, D., Morys, C., Woelfel, J., Cahill, B., Böttcher, M. E., Forster, S., Leipe,
 624 T., Rehder, G., and Neumann, T.: Ecological ReGional Ocean Model with vertically resolved sediments
 625 (ERGOM SED 1.0): coupling benthic and pelagic biogeochemistry of the south-western Baltic Sea,
 626 Geoscientific Model Development, 12, 275-320, 10.5194/gmd-12-275-2019, 2019.



627 Ratmaya, W., Laverman, A. M., Rabouille, C., Akbarzadeh, Z., Andrieux-Loyer, F., Barillé, L., Barillé,
 628 A.-L., Le Merrer, Y., and Souchu, P.: Temporal and spatial variations in benthic nitrogen cycling in a
 629 temperate macro-tidal coastal ecosystem: Observation and modeling, *Cont. Shelf Res.*, 235,
 630 10.1016/j.csr.2022.104649, 2022.

631 Rich, J. J., Arevalo, P., Chang, B. X., Devol, A. H., and Ward, B. B.: Anaerobic ammonium oxidation
 632 (anammox) and denitrification in Peru margin sediments, *J. Mar. Syst.*, 207,
 633 10.1016/j.jmarsys.2018.09.007, 2020.

634 Sayama, M., Sohma, A., and Takasugi, Y.: Experimental analysis of the effect of flow velocity on oxygen
 635 dynamics near the water-sediment interface in a coastal zone., *Proceedings of Coastal Engineering*, 49,
 636 996-1000, 10.2208/proce1989.49.996, 2002.

637 Soetaert, K., Herman, P. M. J., and Middelburg, J. J.: A model of early diagenetic processes from the
 638 shelf to abyssal depths, *Geochim. Cosmochim. Acta*, 60, 1019-1040, 10.1016/0016-7037(96)00013-0,
 639 1996.

640 Sun, L., Wang, C., Yu, H., Liu, D., Houlton, B. Z., Wang, S., Zeng, X., Bai, E., Fang, Y., and Jia, Y.:
 641 Biotic and Abiotic Controls on Dinitrogen Production in Coastal Sediments, *Glob. Biogeochem. Cycle*,
 642 35, 10.1029/2021gb007069, 2021.

643 Tada, K.: Primary Production, Nutrients and Nutrient Release from Bottom Sediments in Coastal Water,
 644 *Journal of Water Environment Society of Japan*, 44, 137-141, 2021.

645 Teng, Z. and Lin, X.: Sediment nitrates reduction processes affected by non-native *Sonneratia apetala*
 646 plantation in South China, *Sci. Total Environ.*, 906, 167523, 2024.

647 Thamdrup, B.: New Pathways and Processes in the Global Nitrogen Cycle, *Annual Review of Ecology*,
 648 *Evolution, and Systematics*, 43, 407-428, 10.1146/annurev-ecolsys-102710-145048, 2012.

649 Umlauf, L., Klingbeil, K., Radtke, H., Schwefel, R., Bruggeman, J., and Holtermann, P.: Hydrodynamic
 650 Control of Sediment-Water Fluxes: Consistent Parameterization and Impact in Coupled Benthic-Pelagic
 651 Models, *Journal of Geophysical Research: Oceans*, 128, 10.1029/2023jc019651, 2023.

652 Wang, X. H.: Tide-Induced Sediment Resuspension and the Bottom Boundary Layer in an Idealized
 653 Estuary with a Muddy Bed, *Journal of Physical Oceanography*, 32, 3113-3131, 10.1175/1520-
 654 0485(2002)032<3113:Tisrat>2.0.Co;2, 2002.



655 Wilson, S. T., Al-Haj, A. N., Bourbonnais, A., Frey, C., Fulweiler, R. W., Kessler, J. D., Marchant, H.
 656 K., Milucka, J., Ray, N. E., Suntharalingam, P., Thornton, B. F., Upstill-Goddard, R. C., Weber, T. S.,
 657 Arévalo-Martínez, D. L., Bange, H. W., Benway, H. M., Bianchi, D., Borges, A. V., Chang, B. X., Crill,
 658 P. M., del Valle, D. A., Fariás, L., Joye, S. B., Kock, A., Labidi, J., Manning, C. C., Pohlman, J. W.,
 659 Rehder, G., Sparrow, K. J., Tortell, P. D., Treude, T., Valentine, D. L., Ward, B. B., Yang, S., and
 660 Yurganov, L. N.: Ideas and perspectives: A strategic assessment of methane and nitrous oxide
 661 measurements in the marine environment, *Biogeosciences*, 17, 5809-5828, 10.5194/bg-17-5809-2020,
 662 2020.
 663 Yamamoto, T., Orimoto, K., Asaoka, S., Yamamoto, H., and Onodera, S.-i.: A Conflict between the
 664 Legacy of Eutrophication and Cultural Oligotrophication in Hiroshima Bay, *Oceans*, 2, 546-565,
 665 10.3390/oceans2030031, 2021.
 666 Yang, J.-Y. T., Hsu, T.-C., Tan, E., Lee, K., Krom, M. D., Kang, S., Dai, M., Hsiao, S. S.-Y., Yan, X.,
 667 and Zou, W.: Sedimentary processes dominate nitrous oxide production and emission in the hypoxic
 668 zone off the Changjiang River estuary, *Sci. Total Environ.*, 827, 154042, 2022.
 669 Yi, Y., Gao, Y., Wu, X., Jia, W., and Liu, Q.: Modeling the effect of artificial flow and sediment flux on
 670 the environment and plankton of an estuary, *International Journal of Sediment Research*, 38, 335-348,
 671 <https://doi.org/10.1016/j.ijsrc.2023.02.001>, 2023.
 672 Zhang, X., Ward, B. B., and Sigman, D. M.: Global Nitrogen Cycle: Critical Enzymes, Organisms, and
 673 Processes for Nitrogen Budgets and Dynamics, *Chem Rev*, 120, 5308-5351,
 674 10.1021/acs.chemrev.9b00613, 2020.
 675 Zhang, X., Zhang, Q., Yang, A., Hou, L., Zheng, Y., Zhai, W., and Gong, J.: Incorporation of microbial
 676 functional traits in biogeochemistry models provides better estimations of benthic denitrification and
 677 anammox rates in coastal oceans, *Journal of Geophysical Research: Biogeosciences*, 123, 3331-3352,
 678 2018.
 679 Zhou, F., Gao, X., Zhang, Y., Yuan, H., Song, J., Liu, K., Yang, B., and Zhuang, W.: Potential mobility
 680 of inorganic nutrients and its controls at the sediment-water interface in the main path of Kuroshio
 681 Current off eastern Taiwan, *Mar Pollut Bull*, 119, 270-276, 10.1016/j.marpolbul.2017.04.002, 2017.



682 Zhou, N., Zhang, G. L., and Liu, S. M.: Nutrient exchanges at the sediment-water interface and the
683 responses to environmental changes in the Yellow Sea and East China Sea, Mar Pollut Bull, 176, 113420,
684 10.1016/j.marpolbul.2022.113420, 2022.
685 Zhu, J., Guo, X., Shi, J., and Gao, H.: Dilution characteristics of riverine input contaminants in the Seto
686 Inland Sea, Mar. Pollut. Bull., 141, 91-103, 10.1016/j.marpolbul.2019.02.029, 2019.
687
688